Journal of Catalysis 270 (2010) 224–233

Contents lists available at ScienceDirect

Journal of Catalysis

journal homepage: www.elsevier.com/locate/jcat

Synthesis and characterization of Au–Pd/SiO_2 bimetallic catalysts prepared by electroless deposition

Jayakiran Rebelli, Michael Detwiler [1], Shuguo Ma, Christopher T. Williams, John R. Monnier *

Department of Chemical Engineering, University of South Carolina, 2C02 Swearingen Engineering Center, 301 S. Main Street, Columbia, SC 29208, USA

ARTICLE INFO

Article history:
Received 23 October 2009
Revised 28 December 2009
Accepted 30 December 2009
Available online 1 February 2010

Keywords:
Electroless deposition
Au electroless bath
Au–Pd bimetallic catalysts
Propylene hydrogenation

ABSTRACT

A series of Au–Pd/SiO_2 catalysts have been prepared by the electroless deposition of Au onto a Pd/SiO_2 catalyst. A kinetically stable, electroless bath consisting of $Au(CN)_2^-$ and N_2H_4 (i.e., Au source and reducing agent) was developed and optimized, allowing for incremental coverages of Au on Pd to be obtained, while avoiding deposition onto the SiO_2 support. The structural and electronic properties of the catalysts were characterized using hydrogen titration of oxygen-precovered Pd, scanning transmission electron microscopy with energy dispersed X-ray spectroscopy, Fourier transform infrared spectroscopy, and X-ray photoelectron spectroscopy. The results suggest that Au was deposited on all types of Pd surface sites (e.g., planes, steps, kinks, edges) in a non-discriminatory fashion, with a net electron transfer from Pd to Au. The catalysts were evaluated for propylene hydrogenation, revealing significantly enhanced turnover frequencies at elevated fractional coverage of Au on Pd ($\theta_{Au} \geqslant 0.60$). The enhanced catalytic activity can be explained by the disruption of continuous Pd ensembles by Au deposition, which prevents formation of the multiply bonded and less reactive propylidyne, while permitting formation of highly reactive and weakly π-bonded propylene.

1. Introduction

Transition metals are often combined to form bimetallic catalysts that have enhanced or unique catalytic properties for various industrial and environmental processes [1]. Often, these supported bimetallic catalysts are prepared either by precipitation or by impregnation routes. However, such methods often do not effectively control the distribution or homogeneity of metals on the substrate, which directly affects the catalytic performance [2]. For the case of Au–Pd bimetallic catalysts, many alternative preparation methods have been used, owing to the importance of these catalysts for CO oxidation, vinyl acetate synthesis, hydrodesulfurization reactions, selective oxidation of alcohols to aldehydes or ketones, alkenes to epoxides, and oxidation of hydrogen to hydrogen peroxide [3–14]. Simultaneous reduction of soluble Au and Pd salts by alcohols (such as ethanol, ethylene glycol, or glycerol) in the presence of polyvinylpyrrolidone (PVP) to prevent agglomeration of the suspended, colloidal metal particles has been used to prepare supported Au–Pd catalysts [14–16]. Comparison of catalysts produced in this manner with those prepared by incipient wetness and co-impregnation methods, indicated that formation of Au–Pd bimetallic alloy catalysts was favored by the PVP method [14,15]. However, calcination at 400 °C was required to completely remove the PVP component; such high temperatures may have adverse effects on morphology and surface composition of bimetallic particles. Regardless, this preparation method has produced catalysts exhibiting higher activities for hydrogenation of aromatic ring compounds than either monometallic Pd or Au catalysts, presumably due to the existence of small Pd ensembles by Au-enriched surfaces of Au–Pd alloys [14,15,17–19].

Prati [20–24] has used activated carbon or polyvinyl alcohol (PVA) to immobilize Au–Pd sols prepared by in situ reduction (using BH_4^-) of solutions containing Au and Pd salts to prepare Au–Pd bimetallic alloys. Despite slight Pd leaching and particle agglomeration, the Au–Pd alloys showed significantly higher activity towards various alcohol oxidation reactions compared to their monometallic counterparts. Ketchie et al. [11] prepared Au–Pd catalysts using a sol-methodology similar to that of Prati, but reported that both bimetallic and monometallic particles were formed. Analysis by EXAFS indicated that for the bimetallic particles preferential coverage of Pd by Au rather than formation of bimetallic alloy particles occurred, indicating a high degree of sensitivity to specifics of the preparative method. Hutchings [25,26] has also extensively used sol-immobilization methods using polyvinyl alcohol (PVA) to synthesize carbon and titania-supported Au–Pd bimetallic alloys; calcination at 400 °C was required to remove the PVA additive from the surfaces of the bimetallic particles.

* Corresponding author. Fax: +1 803 777 8265.
E-mail addresses: rebelli@cec.sc.edu (J. Rebelli), detty87@gmail.com (M. Detwiler), mas@cec.sc.edu (S. Ma), willia84@cec.sc.edu (C.T. Williams), monnier@cec.sc.edu, monnier@engr.sc.edu (J.R. Monnier).
[1] Present address: Dept. of Chemical Engineering, Youngstown State University, One University Plaza, Youngstown, OH 44555, USA.

0021-9517/$ - see front matter © 2010 Elsevier Inc. All rights reserved.
doi:10.1016/j.jcat.2009.12.024

The TiO_2-supported particles consisted of a Pd-rich shell over a Au-rich core, while the carbon-supported particles were homogeneous alloys. Both catalysts were more active for benzyl alcohol oxidation than bimetallic catalysts prepared by impregnation methods [27].

The above-mentioned routes for preparation of Au–Pd catalysts can be considered as bulk methods, where predetermined weights of Au and Pd salts are combined to form bulk particles that combine the two components in either some type of layered structure or an alloy (or both types) of the desired composition. When coupled with the high calcination temperatures needed to completely remove the organic binders (PVA, PVP, ethylene glycol, etc.), the final surface may not reflect the optimum, or intended, surface composition to give the desired activity or selectivity for a particular catalytic reaction. Electroless deposition (ED) is a preparative methodology that provides a way to catalytically deposit in a controlled manner a second metal only on the surface of a pre-existing metallic surface (i.e., not on support) [28–33]. Thus, bimetallic surface compositions can be more effectively controlled to permit more precise correlation of catalyst composition with performance [33] using much lower amounts of the second metal. For example, using sol-immobilization methods to produce a supported 1 wt.% (Au + Pd) catalyst [26], 0.65 wt.% Au was used. However to prepare a Au–Pd catalyst by ED of Au using a 2 wt.% Pd/SiO_2 as the base catalyst, only 0.5 wt.% Au was required to give 50% coverage of the Pd surface by Au (Fig. 6 in this manuscript). In addition, bimetallic catalysts prepared by ED do not require high-temperature calcination and/or reduction treatments, thus avoiding high-temperature restructuring effects. Moreover, this method is applicable for the preparation of virtually all bimetallic compositions [30] as long as the overall redox reaction of the reducible metal salt by the reducing agent is thermodynamically favorable.

Previously, we have used ED to deposit a variety of metals, including Ag, Cu, and Pt on supported monometallic Pt, Pd, Co, and Ru catalysts [28,29,32,33]. In each case, it has been necessary to formulate ED baths that contain a suitable reducing agent, reducible metal salt, and optional salt stabilizer, that are kinetically stable, yet reactive enough to deposit a metal onto the pre-existent, monometallic catalyst surface. These electroless baths have been formulated for the deposition of both partial and multiple metal layers. Bimetallic catalysts such as Ag–Pt/SiO_2 [33] and Cu–Pd/SiO_2 [32] have shown improved performance for selective hydrogenation of 3,4-epoxy-1-butene (EpB), a highly functional olefin. In the case of electrocatalysts for PEM fuel cells, ED-derived Pt–Co/C and Pt–Pd/C catalysts have allowed for more efficient use of the expensive Pt component and higher oxygen reduction activity for the case of Pt–Co/C [28,29].

The present communication focuses on the synthesis of Au–Pd/SiO_2 bimetallic catalysts using electroless deposition methods. The paper describes the development and formulation of a stable and selective Au electroless bath (EB) composition, using $Au(CN)_2^-$ as the Au source and N_2H_4 as the reducing agent. The ED bath is tuned to give mostly catalytic deposition of Au on the Pd surface. However, once the primary metal (Pd) surface is diluted enough by Au, autocatalytic deposition of Au on Au surfaces becomes dominant. Thus, a series of Au–Pd/SiO_2 bimetallic catalysts have been prepared with incremental coverages of Au on Pd. The extent of deposition and the surface distribution of Au have been determined using chemisorption, high-resolution scanning transmission electron microscopy (STEM), energy dispersed X-ray spectroscopy (EDS), Fourier transform transmission infrared (FTIR) spectroscopy of adsorbed CO, and X-ray photoelectron spectroscopy (XPS). The catalysts have also been evaluated for simple olefin (propylene) hydrogenation as a probe reaction to better understand the nature of the Au–Pd interaction. Since this reaction is considered to be structure insensitive and catalyzed only by platinum group metals, catalyst performance can be used to determine whether the Au component induces either ensemble and/or electronic effects on the active Pd surface sites.

2. Experimental

2.1. Materials

Potassium dicyanoaurate, $KAu(CN)_2$ (99% purity Au basis, 68 wt.% Au overall), was used as the gold precursor and hydrazine (35 wt.% N_2H_4 solution) as the reducing agent for the electroless bath, both supplied by Sigma–Aldrich. The basic pH conditions were maintained during ED using a NaOH solution (EM Science). De-ionized water (made using Milli™-Q system) was used to prepare all the aqueous solutions. The primary monometallic catalyst used for ED was 1.85 wt.% Pd/SiO_2 (8.6% Pd dispersion) supplied by BASF Catalysts LLC. Palladium dispersion was calculated from the hydrogen titration of oxygen-precovered Pd sites as described in characterization section. The silica support had a surface area of 100 m^2/g with 0.75 cc/g pore volume and an overall particle size of 150–300 μm.

2.2. Catalyst preparation

The optimized electroless bath contained $Au(CN)_2^-$ and N_2H_4 in a 1:30 molar ratio. Typical bath volumes used were 100 ml per gram of monometallic catalyst (see Section 3 for concentration ranges). During ED at room temperature, the bath was continuously stirred and the pH was maintained between 8 and 10 using a concentrated NaOH solution. Liquid samples (~2 ml) were collected and filtered using 5 μm mesh syringe filters at various time intervals to monitor the time-dependent concentration of Au in the EB. The collected liquid samples were analyzed for Au concentration by AA spectroscopy. After the completion of ED (deposition time ~90–120 min), the slurry was filtered and washed repeatedly until all $Au(CN)_2^-$ and other water soluble ligands (e.g., CN^-, etc.) were removed. $Ag(NO)_3$ (1 M) was added to the washed liquid to detect the presence of residual CN^- ions which could form AgCN, a white precipitate. The washed catalyst was dried in vacuum at room temperature and then stored in glass vials at ambient conditions. By varying the initial Au concentration in the electroless baths, a series of Au–Pd/SiO_2 bimetallic catalysts with different Au loadings were synthesized. For comparison, a 2 wt.% Au/SiO_2 sample was prepared using a traditional incipient wetness (IW) method [34]. After impregnation, the sample was dried in a vacuum oven at ~60 °C and then reduced at 200 °C under flowing H_2 for 1 h.

2.2.1. Liquid phase characterization

UV–Visible (UV–Vis) absorption spectra were measured using a Shimadzu UV-2101PC scanning spectrophotometer. The samples (test and reference) were each loaded into a rectangular quartz cuvette of one cm width and three cm length. The sample measurement was made with respect to a reference scan of the solvent (i.e., water) at pH 9.0. The sample holder was equipped with a thermal jacket connected to an external chiller so that both test and reference cuvette temperatures could be controlled effectively. A small magnetic stirrer was rotated inside the cuvette to maintain realistic ED conditions.

Atomic absorption (AA) spectroscopy was performed on a Perkin–Elmer 3300 and used to determine the elemental concentrations of Au, Pd and Si during ED. In addition, the weight percentages of metals in the final bimetallic catalysts were also determined by digesting 0.04 g of sample in aqua regia at 120 °C for 4 h and then diluting (~20 times) with DI water before analysis. A set of standards (known concentration of each specific element)

was prepared to calibrate the instrument before the actual measurements were made.

2.3. Catalyst characterization

Chemisorption using hydrogen pulse titration of oxygen-precovered Pd was performed using a Micromeritics Autochem II 2920 automated chemisorption analyzer to determine the concentration of surface Pd sites following ED of Au. Prior to titration, approximately 0.1 g sample was reduced in flowing 10% H_2 at 200 °C for 2 h, then exposed to 100% Ar flow for 1 h at 200 °C to remove chemisorbed hydrogen from the metal surface. After cooling to 40 °C in flowing Ar, the sample was exposed to 10% O_2/balance Ar for 30 min to saturate the Pd surface with adsorbed atomic oxygen. Following exposure to 100% Ar for 30 min to remove residual O_2, the sample was ready for pulse flow H_2 titration. At room temperature the adsorbed atomic oxygen reacts rapidly with the 10% H_2/balance Ar pulse (pulses repeated at 4 min intervals) to form H_2O and replace the adsorbed oxygen atom with atomic hydrogen. Hydrogen consumption was quantitatively determined by means of a high sensitivity thermal conductivity detector below the sample cell. Hydrogen pulses were continued until no further uptake of H_2 was observed. Hydrogen titration of O-precovered Pd was used rather than H_2 chemisorption because of problems associated with formation of bulk β-palladium hydrides; likewise, chemisorption of CO was not used due to uncertainties of CO/surface Pd stoichiometry. At the timescale used for H_2 pulse titrations, H_2 rapidly reacts with adsorbed O atoms to form H_2O and to cover the vacant Pd site with atomic H without formation of β-palladium hydride [35].

FTIR spectroscopy was used to detect adsorbed CO on the metal surface. Spectra were collected using a Thermo Electron model 4700 FTIR spectrometer with a liquid nitrogen-cooled MCT detector. In these measurements, a 0.015 g sample was pelletized into a disk of 1 cm diameter, and then placed in a temperature-controlled flow cell [32,33]. The samples were reduced in H_2 for 1 h at 200 °C, cooled to 25 °C in He, and then exposed to 1% CO in He. After 30 min, the flow cell was purged with pure He to remove any physisorbed and gas-phase CO. All the spectra were referenced to an initial background spectrum taken prior to CO exposure. The FTIR spectra were analyzed and the peaks were resolved using Peaksolve software (Galactic). The spectra were initially baseline corrected, and during peak deconvolution, the type of peak, height and width parameters were constrained accordingly.

Scanning transmission electron microscopy (STEM) and energy dispersed X-ray spectroscopy (EDS) were used to determine nanoparticle size distributions and bimetallic compositions, respectively. Measurements were performed using a JEOL 2100F equipped with a CEOS Cs corrector system. High angle annular dark-field (HAADF) STEM images were acquired on a Fischione Model 3000 HAADF detector with a camera length such that the inner cut-off angle of the detector was 50 mrad. A solid-state Si(Li) X-ray detector from Oxford Instruments was used to collect the EDS data. Quantification was made using Inca TEM software which uses theoretical k-factors for its thin film, microanalysis algorithm. Holey-carbon coated Cu grids were dipped into finely powdered catalysts samples for examination under the microscope. The effective particle diameter was calculated assuming spherical particles by measuring the surface area of bright spots on the captured dark-field images. If the particle had irregular or chain-like structures, the surface was divided into multiple particles at the observable grain boundaries. Several images at different locations were captured for each catalyst sample to measure overall effective surface area/particle size distribution. For all histograms, a minimum of 60–80 particles were measured.

X-ray photoelectron spectroscopy measurements were carried out on a Kratos AXIS Ultra DLD XPS system equipped with a hemispherical energy analyzer and a monochromatic Al Kα source. The Al Kα source was operated at 15 keV and 150 W, incident at 45° with respect to the surface normal. The pass energy was fixed at 40 eV for the detailed scans. The samples were reduced at 200 °C for 1 h and cooled to 25 °C in Ar, using a separate catalysis cell in a controlled environment. Since the SiO_2 support is an insulator, a charge neutralizer was used to compensate the substrate charge during XPS measurements. All spectra were corrected using 103.4 eV as a reference for Si 2p binding energy (BE). The spectra were fitted to a Shirley–Linear background using XPSPEAK software version 4.1. Appropriate peak positions and area constraints were used for peak splitting of 4f and 3d electrons. The FWHM was maintained constant at ~1 eV for Pd 3d and Au 4f electrons.

2.4. Kinetic evaluation

Propylene hydrogenation reaction studies were carried out in a thermostatically jacketed, tubular stainless steel reactor to maintain low reaction temperatures (0–15 °C). The internal diameter of the reactor was 0.19 in. Approximately 20 mg of catalyst diluted with 2 g of SiO_2 was supported on glass wool in the reactor. The catalyst was prereduced at 200 °C in 10% hydrogen for an hour and cooled down to 10 °C to initiate the reaction. A mixture of 5% propylene, 20–95% hydrogen and balance helium was fed to the reactor at 400 SCCM and one atm overall reaction pressure. The reactor feed and products were analyzed using in-line sampling methods and an HP 5890 gas chromatograph equipped with a thermal conductivity detector. Reaction rates, feed conversions, and turnover frequencies (TOFs) were calculated and compared for both monometallic and bimetallic systems.

3. Results and discussion

3.1. Electroless bath development

To electrolessly deposit a second metal (i.e., Au) onto a monometallic catalyst, a thermodynamically unstable, but kinetically stable, electroless bath is required. A typical electroless bath is made up of a metal source, reducing agent, and solvent (typically water) [29,33]. In some cases, the bath is modified by addition of other chemical reagents to improve the stability, efficiency and/or to provide better control over deposition kinetics. A wide variety of gold electro-deposition and autocatalytic ED baths are commercially available due to their extensive use in electronic/semiconductor coating applications [30,36–43]. In the case of catalyst synthesis, the applicability of the ED bath depends on various factors like concentrations of metal ion source, reducing agent, monometallic catalyst, pH, and temperature since the goal is to have controlled rates and amounts of the metal to be deposited.

3.1.1. Choice of metal sources and reducing agents

The present EB is configured using potassium dicyanoaurate, $KAu(CN)_2$ as the Au source. The negative standard reduction potential for $Au(CN)_2^-$ ($E^o_{Au(CN)_2^-} = -0.60$ V) is favorable for the formation of kinetically stable electroless solutions with long life times. In addition to stability, $Au(CN)_2^-$ is resistant to galvanic deposition of Au on Pd. In order to reduce the stable $Au(CN)_2^-$ ion to metallic Au, a relatively strong reducing agent such as hydrazine is used [44]. The choice of reducing agent may also influence the type of deposition (i.e., catalytic or autocatalytic) that will occur, and thus the surface morphology and structure of the deposit [45,46]. During the initial step of electroless deposition, the monometallic (Pd) catalyst surface activates the reducing agent. For the metals considered here, Au has a higher oxidation capability compared to Pd, which should result in catalytic deposition of Au on the Pd

surface being favored at submonolayer coverages of Au. At latter stages of ED, as the Pd surface becomes covered by Au, both catalytic and autocatalytic ED deposition will likely occur [47–49].

3.1.2. Bath stability and kinetics of deposition

One of the most important aspects of an electroless bath is its kinetic stability, or the ability to maintain the secondary metal in a positive oxidation state in an aqueous solution during the time period it is being catalytically reduced onto the primary metal. The electroless bath becomes kinetically unstable when the soluble Au^+ is reduced to metallic Au° in solution before being electrolessly deposited on the pre-existing metal surface.

To determine bath stability and possible formation of Au° in solution, UV–Visible spectroscopy was used. Typically, Au particles <10 nm yield a pink/purple, colored solution with a broad UV–Visible absorption band between 500 and 650 nm [36,50,51]. Fig. 1 shows a typical set of time-dependent UV–Visible spectra for a $Au(CN)_2^-/N_2H_4$ bath at room temperature and pH 9. The transition from a stable solution to an unstable one is first observed as a broad peak emerging from 530 to 700 nm after 24 h of bath lifetime. After 36 h, the bath becomes completely unstable with large Au agglomerates exhibiting a dark pink/purple, colored solution with a high intensity peak. Because the amount of Au deposition is dependent on the concentration of $Au(CN)_2^-$ in solution, the stability of ED bath at various concentrations of $Au(CN)_2^-$ (at constant N_2H_4 concentration) is summarized in Fig. 2. The results indicate that $Au(CN)_2^-$ concentrations $\leqslant$0.045 mM are stable for at least 24 h and should function as stable ED baths, even when the concentration of N_2H_4 is two orders of magnitude greater than the $Au(CN)_2^-$ concentration.

The kinetic dependencies of $Au(CN)_2^-$, N_2H_4, and surface Pd site concentrations for Au deposition were also examined in more detail. The data for $Au(CN)_2^-$ dependency are summarized in Figs. 3 and 4. The deposition curves in Fig. 3 indicate that SiO_2 alone does not result in deposition of Au, but that Pd is required for catalytic deposition. While not so obvious from Fig. 3, higher concentrations of $Au(CN)_2^-$ in solution give more rapid rates of deposition. This is shown in Fig. 4, and application of the power rate law formalism indicates approximately first order dependency for $Au(CN)_2^-$. Likewise, kinetic dependencies for N_2H_4 and Pd surface site concentrations are shown in Figs. 5 and 6, respectively. In all cases, to obtain true deposition rates of Au on Pd, only initial rates were used in order to avoid contributions from autocatalytic deposition of Au. The results indicate Au deposition is essentially zero order for N_2H_4 concentration and approximately 0.5 order for Pd surface site concentration. The kinetic dependencies are consistent with the

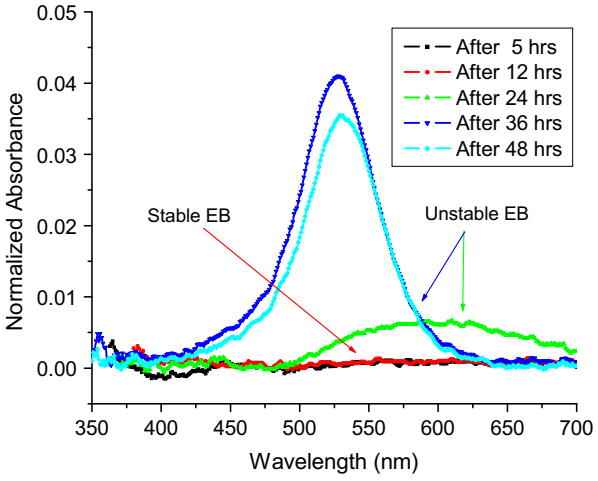

Fig. 1. Time-dependent UV–Visible spectra at 25 °C: $[Au(CN)_2^-] = 0.1$ mM, $[N_2H_4] = 3.0$ mM, and pH 9.

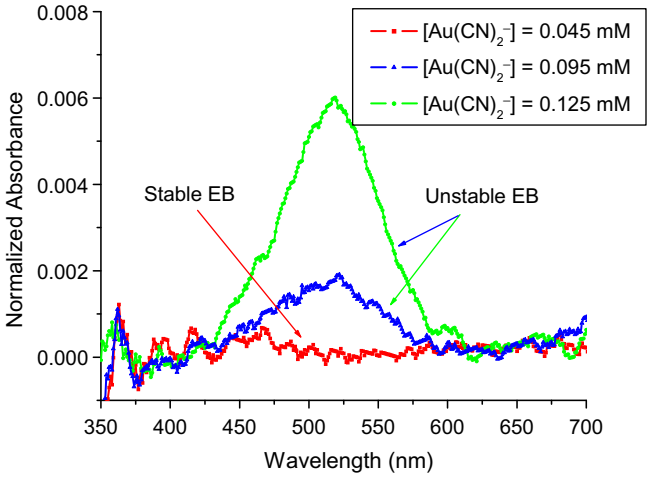

Fig. 2. UV spectra of EB at 25 °C with increasing $Au(CN)_2^-$ concentrations at constant $[N_2H_4] = 5.0$ mM at pH 9 after 24 h of lifetime.

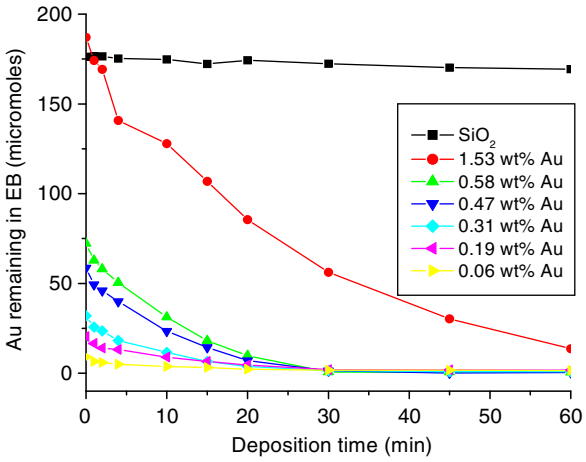

Fig. 3. Au deposition profiles for synthesis of Au–Pd/SiO_2. The legend denoted the weight percent of Au deposited on the silica-supported Pd particles. The SiO_2 blank was the same as the SiO_2 support for Pd.

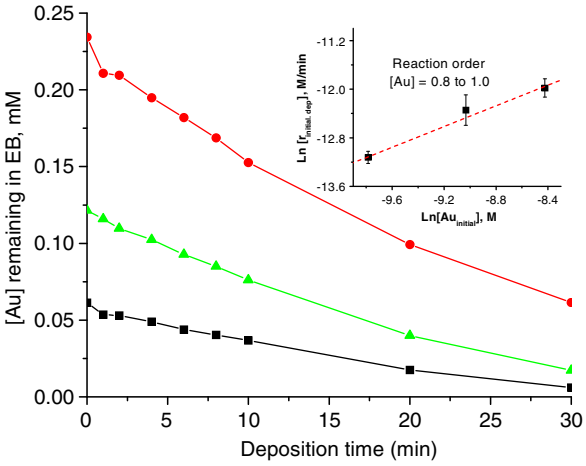

Fig. 4. Reaction order dependency for $Au(CN)_2^-$, at constant $[N_2H_4] = 3$ mM, 0.5 g Pd/SiO_2, and pH 9.

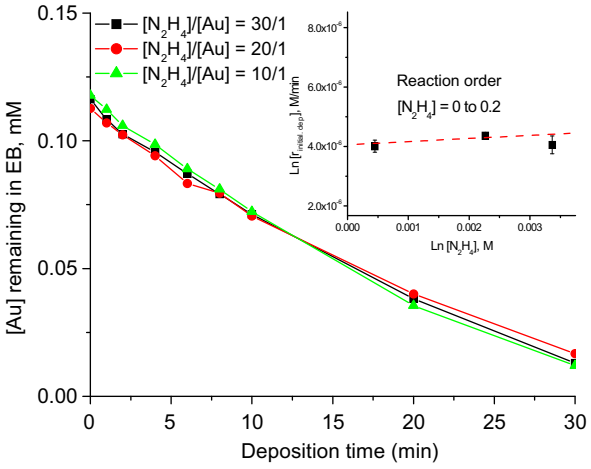

Fig. 5. Reaction order dependency for N_2H_4 at constant [Au] = 0.1 mM, 0.5 g Pd/SiO_2, and pH 9.

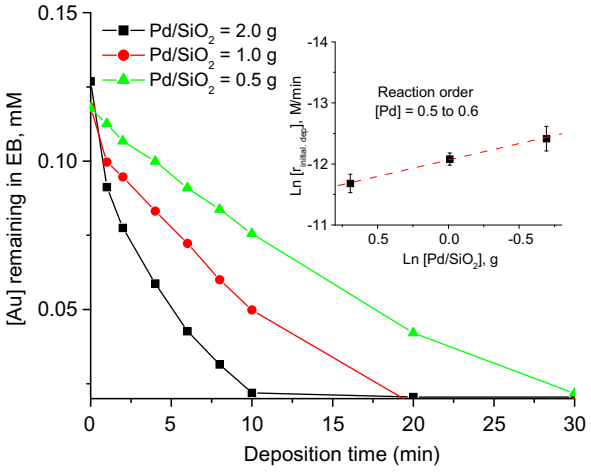

Fig. 6. Reaction order dependency for Pd concentration at constant $[Au(CN)_2^-] = 0.1$ mM, $[N_2H_4] = 3$ mM, and pH 9.

reactivities of the individual components; $Au(CN)_2^-$ is a thermodynamically stable species and reduction of this anion should be the slowest step, as indicated by the near first order dependency. Conversely, the activation of N_2H_4, considered to be a relatively strong reducing agent, should be quite facile and, not surprisingly, exhibits a near zero order dependency. The half-order dependency for Pd site concentrations is not obvious, but may indicate two Pd sites are required for Au^+ reduction and deposition. While hydrazine can be considered a four electron donor in alkaline baths, it may also consume two electrons to form ammonia [52]. As such, higher concentrations of hydrazine are recommended for reasonable Au deposition rates. The optimal $N_2H_4 : Au(CN)_2^-$ molar ratio for desirable ED rates, while maintaining kinetic stability, was chosen to be ~20:1 for the preparation of the Au–Pd bimetallic catalysts in this study, even though $Au(CN)_2^-$ offers a relatively wide stability range due to its high negative reduction potential.

Finally, the choice of solution pH is critical, not only for determining the kinetics of electroless deposition, but to suppress electrostatic adsorption of $Au(CN)_2^-$ on the SiO_2 surface. The formation of true bimetallic catalysts requires that ED occurs only on the catalytic Pd sites and not on the SiO_2 support. This surface charge-based interaction between $Au(CN)_2^-$ and SiO_2 can arise if the pH of the solution is below the point of zero charge (PZC) for silica (between 2 and 6 [53]). Thus, solution pH > 6 should maintain the SiO_2 in a deprotonated state and minimize interactions with $Au(CN)_2^-$. Even though the rate Au deposition increases with basicity, in this study, the pH was always maintained <10 to prevent gelation of SiO_2 and loss of mechanical stability of the support. Taking all these factors into account, the stable life time and optimized electroless deposition composition are summarized in Table 1.

3.2. Synthesis, characterization, and evaluation of Au–Pd/SiO_2 catalysts

3.2.1. Synthesis

A series of Au–Pd/SiO_2 bimetallic catalysts were prepared to obtain increasing coverages of Au on Pd. The bath concentrations were chosen at kinetically stable conditions such that complete deposition occurs within the first 60 min. Two grams each of the various Au–Pd/SiO_2 catalysts were synthesized at room temperature and pH 9 by varying initial $Au(CN)_2^-$ concentrations. The time-dependent Au deposition profiles are shown in Fig. 3; the catalysts exhibit loadings of up to 2.01 wt.% Au on Pd/SiO_2.

3.2.2. Characterization

To evaluate the effectiveness of the ED process for deposition of Au on Pd, catalysts were characterized by chemisorption using the method of hydrogen titration of oxygen-precovered sites [54,55]. Fig. 7 shows H_2 uptake plotted as a function of Au weight loading as measured using AA spectroscopy. As Au wt.% increases, H_2 uptake decreases linearly up to approximately 0.5 wt.% Au. At higher Au loadings, H_2 uptake decreased only marginally. The solid line in Fig. 7 shows the theoretical H_2 uptake expected for Pd/SiO_2, assuming only catalytic deposition of Au on Pd in a 1:1 Au:Pd surface atomic ratio. In this case, 0.31 wt.% of Au is required for one theoretical monolayer. It is evident from Fig. 7 that the experimental ED profile diverges from the theoretical line even at low Au loadings and that autocatalytic deposition occurs even during the early stages of Au^+ deposition.

According to electrochemical anodic oxidation studies [49], hydrazine should be preferentially oxidized on Pd compared to Au, resulting in catalytic deposition of submonolayer coverages of Au on Pd. However, the presence of CN^- ligands in solution has been shown to enhance autocatalytic deposition of Au [56]. This appears to occur in our case and autocatalytic deposition is observed at early stages of deposition and increases further at higher Au loadings. Of course, autocatalytic deposition should also increase as the concentration of available surface Pd sites decreases (0.5 reaction order for catalytic deposition in Fig. 6).

High-resolution STEM and EDS measurements were performed to measure the particle size distributions and bimetallic particle compositions of selected catalysts. Fig. 8 shows HRTEM images and histograms of the particle size distributions for monometallic Pd/SiO_2 and 2.01 wt.% Au–Pd bimetallic catalysts. For monometallic Pd/SiO_2, approximately 30% of the particles are 4 nm in diameter, while the remaining are scattered over a wide range (up to 30 nm) creating a broad particle size distribution. In addition,

Table 1
Optimized conditions for stable[a] electroless baths at pH 8–10 and 25 °C.

EB component	EB composition
Gold source	$Au(CN)_2^-$ < 0.20 mM
Reducing agent (RA)	$[N_2H_4]$ < 50 mM
Order of RA oxidation capability	Pd > Au

[a] At least 4 h stability.

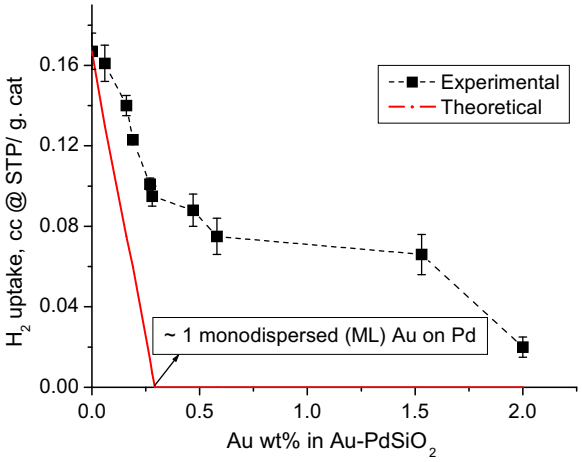

Fig. 7. Chemisorption results using H_2 titration of oxygen-precovered Pd sites.

many of the larger particles are in the form of agglomerates/clusters with irregular, long chain-like structures. For such structures, effective particle diameters were reported. After the addition of Au to Pd, the size distribution is slightly skewed towards large effective particle diameters (see Fig. 8) as expected since the addition of Au to the Pd particles should increase overall particle diameters.

The bimetallic catalyst compositions were examined using EDS for a minimum of eight particles of different size ranges (effective particle diameter varied from 4 to 20 nm as shown in Table 2); all particles showed bimetallic composition. If the rate of Au deposition is independent of Pd particle size, the smaller Pd particles should have higher Au atomic percentages, as observed for particles <4 nm. For larger Pd particles, i.e., 4–20 nm, the bimetallic compositions determined from EDS were similar to the bulk compositions determined by AA spectroscopy. These observations suggest that the Au electroless deposition is independent of Pd surface morphologies and particle sizes.

The bimetallic nanoparticle surfaces were also characterized by FTIR measurements of CO adsorption at 25 °C. The FTIR spectra obtained after 30 min of He purge (to remove residual gas-phase and weakly adsorbed CO [57,58]) are shown in Fig. 9. For both Pd/SiO_2 and Au–Pd/SiO_2 catalysts, CO stretching bands were observed in both 2000–2100 cm^{-1} and 1800–2000 cm^{-1} regions, due to linear and multiply-coordinated CO on Pd sites, respectively [59]. In the case of Pd/SiO_2, the linear region was deconvoluted into two peaks centered at 2077 and 2047 cm^{-1}, which are attributed to linearly bonded CO molecules at low coordination sites (i.e., defects like corners, steps and kinks of Pd(1 1 1) and Pd(1 0 0)) [60,61]. The region between 1800 and 2000 cm^{-1} contains several overlapping features, which are resolved by curve fitting into peaks at 1978, 1938, 1876, and 1812 cm^{-1}. These peaks are associated with CO vibrations arising from bridged and threefold multisite adsorbed species. Specifically, peaks at 1978 and 1938 cm^{-1} can be assigned to twofold, bridged CO species on low index planes such as Pd(1 1 0) and Pd(1 0 0), respectively [59,61–63]. The peaks at 1876 and 1812 cm^{-1} are consistent with CO adsorption on threefold hollow sites on Pd(1 1 1) surfaces [59,64].

In the case of bimetallic surfaces, the intensity of both bridged and linear CO–Pd bands decrease, indicating lower CO uptake due to electroless deposition of Au on Pd. However, the relative intensity ratios of linear, bridged, and threefold hollow CO adsorption peaks were not significantly altered with deposition, suggesting that Au is being indiscriminately deposited on all Pd surface sites. In such a situation, the intensities of all bands would

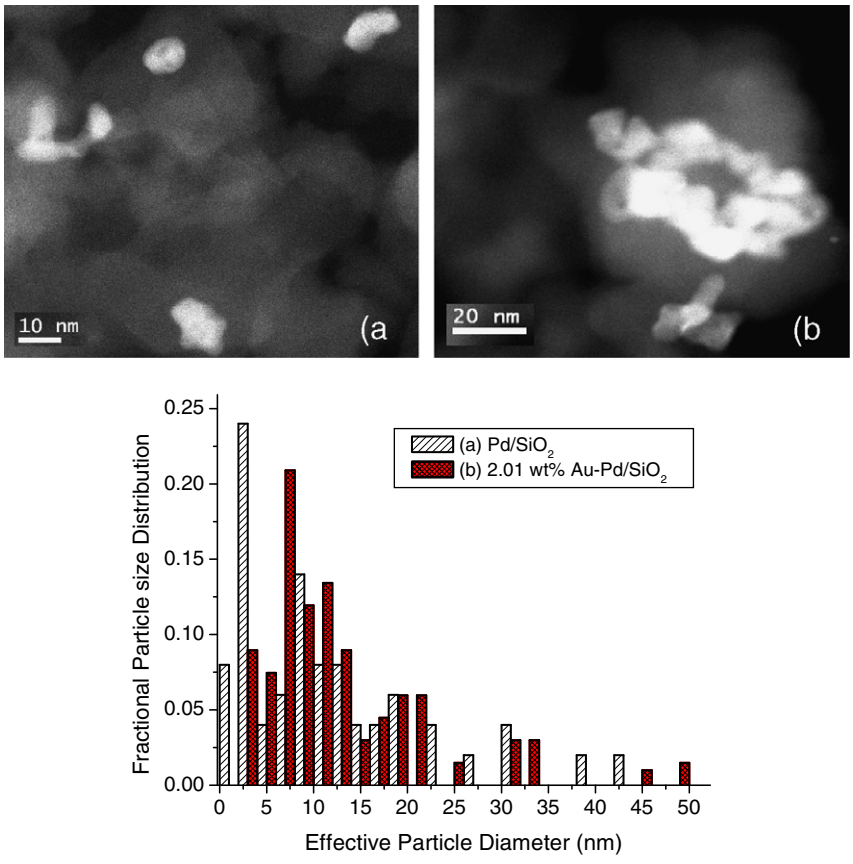

Fig. 8. Particle size distribution of (a) Pd/SiO_2 and (b) 2.01 wt.% Au–Pd/SiO_2.

Table 2
EDS particle compositions for Au–Pd/SiO_2 and comparison to AA* analysis.

Effective particle size (nm)	Atomic composition (%)					
	0.16 wt.% Au–Pd/SiO_2		1.53 wt.% Au–Pd/SiO_2		2.01 wt.% Au–Pd/SiO_2	
	Au	Pd	Au	Pd	Au	Pd
<4	48	52	n/a	n/a	n/a	n/a
4–10	5	95	27	73	40	60
10–20	6	94	25	75	27	73
Bulk composition*	5	95	31	69	37	73

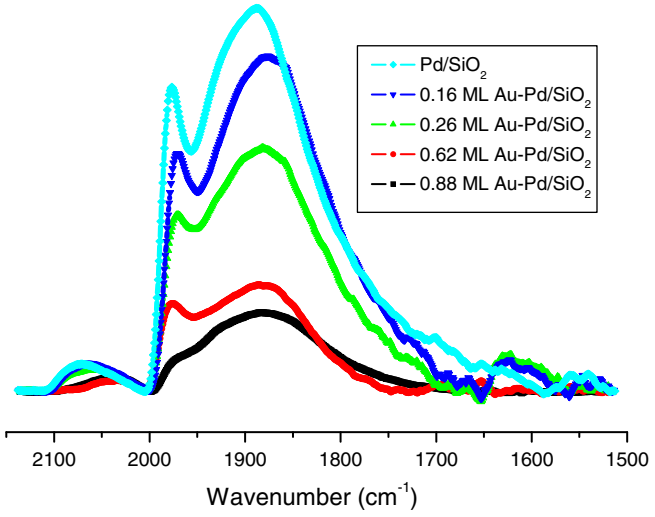

Fig. 9. Transmission FTIR spectra of CO adsorption on monometallic Pd/SiO_2 and bimetallic Au–Pd/SiO_2 catalysts.

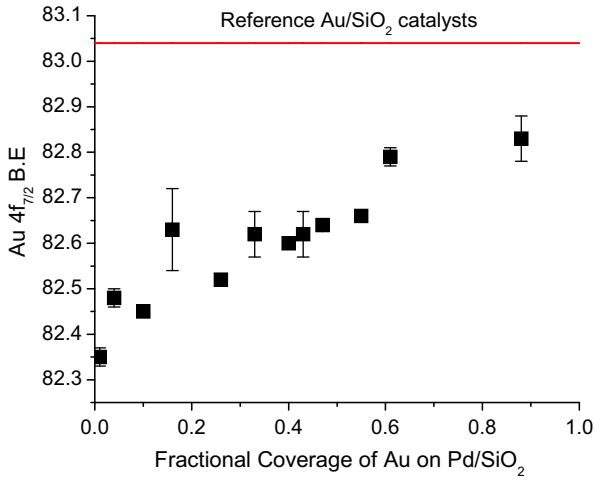

Fig. 10. XPS binding energy for Au $4f_{7/2}$ vs. Au coverage on Pd. Au coverages were determined by chemisorption.

be expected to decrease, but the shape of the spectra would remain roughly constant. Thus, the results suggest that Au electroless deposition on Pd is not particularly favored on any of the various Pd surface planes or other sites (i.e., steps, edges, kinks) that are exposed. These results are in agreement with the recent work of Schaal et al. [32] who also used FTIR of CO to show that ED of Cu^{2+} (using a pH 9 solution with HCHO as the reducing agent) on Pd/SiO_2 also resulted in non-specific deposition on all Pd sites. Thus, the non-discriminatory nature of ED on Pd surfaces may be more due to the nature of Pd rather than the selection of reducing agent or reducible metal ion. In addition to decreases in intensity, FTIR peaks shift by varying degrees (10 cm^{-1} for linear and 25 cm^{-1} for non-linear CO on Pd) to lower frequencies at the highest weight loadings of Au. Such frequency shifts could result from electronic interaction between Pd and Au, as has been reported previously for AuPd alloys [14,15,65,66]. However, it is difficult to rule out other explanations for the shifts, such as decreased dipole coupling due to Pd surface site dilution as reported by Schaal et al. [33] for the Ag–Pt/SiO_2 system.

To explore the possibility of electronic interactions between Au and Pd, XPS measurements were performed and the results were summarized in Fig. 10. For Au, the high intensity $4f_{7/2}$ peak was monitored, while for Pd the less intense $3d_{3/2}$ peak was monitored because the $3d_{5/2}$ peak overlapped with the Au $4d_{5/2}$ peak. At the highest Au loading (2.01 wt.% Au, ~0.88 ML Au), the Au 4f electron binding energy (BE) was ~0.20 eV lower than that for the Au/SiO_2 (~2.0 wt.% Au) reference catalyst. As the Au loadings decreased, the Au 4f BE shifts further from ~82.8 eV downward to 82.3 eV, increasing the negative shift to ~0.8 eV versus the reference Au/SiO_2. However, for the Pd 3d electrons, only a very small shift (<0.1 eV) was observed since relatively few Pd atoms are associated with the deposited Au and contribute to the measured Pd 3d XPS signal; the great majority of the Pd atoms are associated with the bulk of the Pd particle. For bimetallic catalysts, BE shifts could arise from changing particle sizes [67] or electronic interactions [68] between metals. In the present case, the particle size distributions are relatively constant and broad enough for the Pd and Au–Pd catalysts that they can be considered relatively constant for the entire compositional range. Consequently, the observed negative shift with decreasing Au loading is most likely due to electronic interactions, with a net transfer of electron density from Pd to Au.

In addition to BE shifts, the bimetallic surface/near surface compositions were also determined from the XPS measurements. The individual peak intensities were integrated and the atomic ratios of Au/Pd were compared to the surface compositions from chemisorption experiments and the bulk compositions measured by AA (Fig. 11). Since XPS experiments reflect the atomic composition of the top several layers (penetration depth ~5 nm), the autocatalytic deposition of Au on Au should give higher Au/Pd ratios than either chemisorption (surface) or AA (bulk) measurements. Although the ratios mismatch for the bulk and surface compositions, they vary in a near linear manner with Au wt.% loadings up to 0.58 wt.% Au (~50% coverage of Au on Pd obtained by chemisorption analysis). As observed in chemisorption experiments for low Au wt loadings, the deviation of bulk and surface measurements indicates the occurrence of both autocatalytic and catalytic ED processes. At higher Au wt.% loadings (above 0.58 wt.% Au), the autocatalytic process clearly dominates the deposition of Au.

3.2.3. Catalytic evaluation

The Au–Pd/SiO_2 bimetallic catalysts were evaluated using propylene hydrogenation, a structure-insensitive reaction where the catalytic activity of metals has been found to be independent of

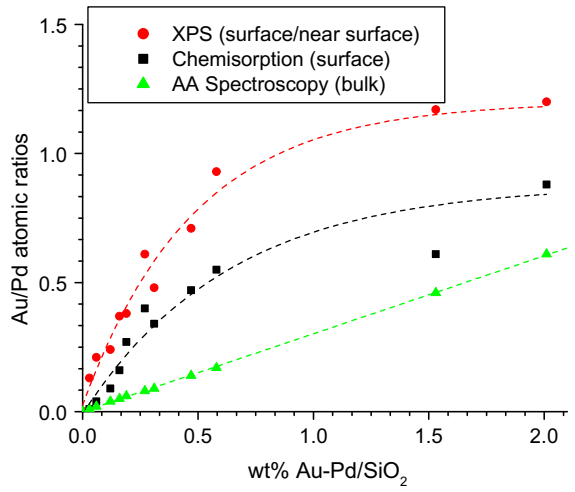

Fig. 11. Au/Pd surface and bulk atomic ratios based on different methods.

particle size and surface structure [69,70]. In order to examine the intrinsic activity of Pd with increasing Au loadings, turnover frequencies (TOFs) for C_3H_6 conversion were calculated using the exposed Pd sites measured by chemisorption. All catalysts deactivated somewhat when brought on stream; thus, turnover frequencies were calculated both initially and after 16 h on stream. Fig. 12 shows TOFs plotted versus coverage of Au on Pd. At lower Au coverages ($\theta_{Au} \leqslant 0.4$), both the initial and 16 h on stream TOF values increased only slightly with Au loading and were quite similar to the values for Pd alone, indicative of a structure-insensitive reaction. By contrast, at Au coverages $\theta_{Au} \geqslant 0.4$, the initial TOF values increased much more steeply; however, after 16 h on-line, much of the higher activity has been lost due to a higher extent of deactivation. Regardless, even after deactivation, the TOFs were still 4–5 times higher than for Pd/SiO_2.

The hydrogenation reaction mechanism proceeds by competitive adsorption of propylene and dissociative adsorption of hydrogen on the Pd surface [71]. The adsorption of propylene is assumed to proceed through a 1,2-di-σ bonded species that undergoes stepwise hydrogenation to form propane. However, if insufficient adsorbed hydrogen is available to rapidly hydrogenate the di-σ species to propane or if the surface geometry of Pd ensembles permits, the di-σ bonded propylene may undergo dehydrogenation to form more propylidene and, consecutively, propylidyne. Both terminally bonded species are very stable and strongly bound to the

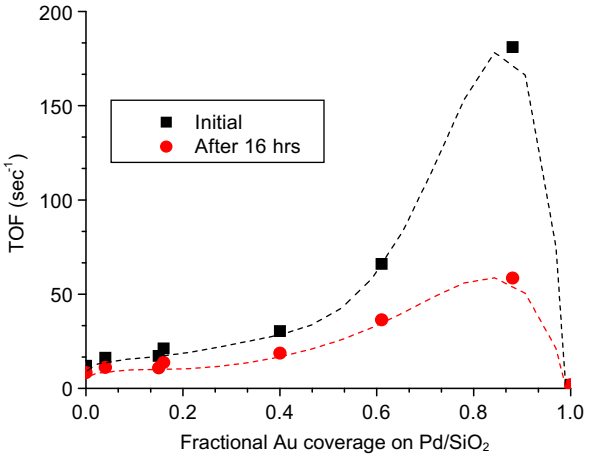

Fig. 12. Hydrogenation of propylene on 2.01 wt.% Au–Pd/SiO_2@400 SCCM, 10 °C, feed: 5% C_3H_6 20% H_2 balance He.

Pd surface with propylidyne preferably bonded in threefold hollow sites on the (1 1 1) surface. By extension from the work of Somorjai and coworkers [72–74] for the hydrogenation of ethylene on Pt surfaces, the formation of a more weakly, π-bonded propylene in an atop position on Pt or Pd sites is more likely to be the active species for hydrogenation of propylene. Somorjai noted that the rate of hydrogenation of π-bonded ethylene was 10^6 times higher than for ethylidyne and that because the di-σ bonded ethylene was competitively and unfavorably adsorbed with ethylidyne on the same threefold sites, it actually played only a minor role in ethylene hydrogenation. If we extrapolate from ethylene to propylene, we may also conclude that π-bonded propylene is the key intermediate in propylene hydrogenation. In this context, we can better explain the effects of high Au coverages on the Pd surface. At high fractional coverages of Au on Pd, the Pd surface is broken into ensembles that prevent formation of the multiply bonded and less reactive propylidyne while permitting formation of the highly reactive and weakly π-bonded propylene. Note that deviation from structure insensitivity is only observed at $\theta_{Au} \geqslant 0.6$; at these coverages the Pd ensemble sizes are quite small, particularly for the $\theta_{Au} = 0.88$ sample.

The earlier results for FTIR of CO indicated that Au deposition was essentially non-discriminatory; thus, Au deposition occurs on all Pd surface sites. We can also rule out the possibility that Au migration or surface restructuring occurs at the reaction conditions of 0–20 °C since all catalysts were pretreated at 200 °C in H_2/He for 2 h prior to reaction; these pretreatment conditions were identical to those used before chemisorption measurements were made for the $Au–Pd/SiO_2$ samples.

We cannot rule out the possibility that the structure sensitivity may be due to electronic effects since the XPS results indicated transfer of e^- density from Pd to Au. The formation of e^--deficient Pd sites may result in preferential electrophilic attack at the e^--rich C═C double bond of propylene to favor the formation of π-bonded propylene. However, this effect should result in a linear increase in activity with Au coverage, not the abrupt increase in activity at $\theta_{Au} \geqslant 0.6$. The formation of Au-induced Pd ensembles provides a better explanation for the observed reactivity trends.

Catalyst deactivation can also be explained by the existence of Pd ensembles. While the formation of π-bonded propylene is favored for the ultra small Pd ensembles, sites available for dissociative H_2 adsorption become limited. At these conditions, extended lifetime of the adsorbed C_3H_6 species may lead to the formation of propylene oligomers that are unreactive at conditions of low temperature and low H_2 partial pressures [73,75]. This type of surface fouling should be more dramatic for smaller Pd ensembles than unmodified Pd or low Au loading surfaces, since the availability of Pd surface sites for H_2 adsorption is much more limited. The Pd site concentration for Pd/SiO_2 is approximately 8.5 times higher for the unmodified Pd catalyst than the $\theta_{Au} = 0.88$ sample. Consistent with carbon-based fouling, complete activity could be restored after 20% O_2 post treatment for 1 h at 100 °C.

To determine whether higher H_2 partial pressures would lower the extent of deactivation, the reaction was conducted over the P_{H_2} range 0.05–0.95 atm for both Pd/SiO_2 and 2.01 wt.% $Au–Pd/SiO_2$ ($\theta_{Au} = 0.88$ sample); the results are shown in Fig. 13. Deactivation for Pd/SiO_2 was essentially independent of H_2 partial pressure, indicating that the formation of strongly bound propylene species such as propylidene and propylidyne controlled the extent of fouling. However, for the $Au–Pd/SiO_2$ sample, deactivation was greatly suppressed by increasing the H_2 concentration from 5% to 95%, consistent with the formation of small Pd ensembles for the Au-modified Pd catalyst. The higher H_2 pressures permit adequate surface concentrations of hydrogen on the Pd surface to readily hydrogenate the weakly bound propylene species. The combination of very small, Au-induced Pd ensembles and higher H_2 pressures

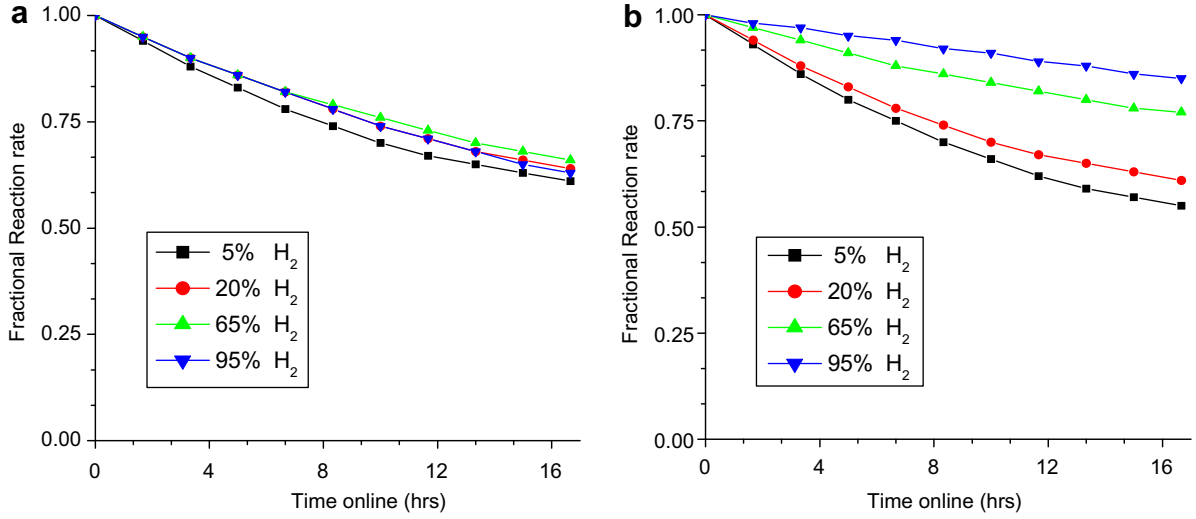

Fig. 13. Hydrogenation of propylene on (a) Pd/SiO_2 and (b) 2.01 wt.% $Au–Pd/SiO_2$@400 SCCM, 10 °C, with varying feed: 5% C_3H_6 5–95% H_2 balance He.

results in the formation of a stable, reactive catalyst for propylene hydrogenation.

4. Conclusions

It has been shown that $Au–Pd/SiO_2$ catalysts with incremental coverages of Au on Pd can be prepared using electroless deposition of Au onto a Pd/SiO_2 catalyst. A kinetically stable, electroless bath consisting of $Au(CN)_2^-$ and N_2H_4 was developed and optimized in order to selectively deposit the Au on Pd (as opposed to the SiO_2 support), while avoiding formation of undesired Au clusters/nanoparticles in solution. Characterization of ED-derived catalysts using hydrogen titration of oxygen-precovered Pd, STEM with EDS, FTIR, and XPS reveal several features of the ED process and bimetallic catalyst structure. Hydrogen titration of oxygen revealed that ED proceeds via both catalytic (Au on Pd) and autocatalytic (Au on Au) pathways in the initial stages, with the latter pathway dominating at high fractional Au coverages ($\theta_{Au} \geqslant 0.50$). The catalytically deposited Au was found to deposit on all types of Pd surface sites (e.g., planes, steps, kinks, edges) in a non-discriminatory fashion, as adjudged by the results of STEM/EDS and FTIR measurements. Finally, XPS measurements are consistent with the above-mentioned conclusions, and reveal a net electron transfer from Pd to Au that varies with the extent of Au loading.

The catalytic performance of these catalysts was evaluated for propylene hydrogenation, which is typically a structure-insensitive reaction. However, it was found that elevated fractional coverages of Au on Pd ($\theta_{Au} \geqslant 0.60$) resulted in enhanced TOFs for this reaction. Such enhanced rates are a result of Au-disrupted Pd atom ensembles, which prevent formation of multiply bonded and less reactive propylidyne, while permitting formation of highly reactive and weakly π-bonded propylene. The higher degree of deactivation in these very active bimetallic catalysts can also be explained by disrupted Pd ensembles. Such small ensembles have decreased capability for dissociative H_2 adsorption, resulting in more surface fouling than for unmodified Pd or low Au-loaded surfaces.

Overall, the results reported here further demonstrate that ED provides an avenue to rationally prepare bimetallic catalysts with controlled composition. Indeed, the present interesting (and perhaps unexpected) catalytic results for propylene hydrogenation show the enhanced fundamental insight that can be obtained by systematically preparing a wide range of bimetallic compositions with relatively small increments of surface coverage. This promising method is thus now being employed by our group to prepare bimetallic catalysts for a variety of catalytic reactions (e.g., liquid phase oxidation of glycerol) relevant to production of renewable fuels and chemicals.

Acknowledgments

This research project was supported financially by an NSF Collaborative Research Grant (CBET 0854339) and REU site Grant (EEC 0552702), as well as the University of South Carolina Nanocenter. The authors also thank BASF LLC for supplying Pd/SiO_2 catalysts for these studies. We also thank the USC Electron Microscopy Center and Dr. Douglas Blom for assisting with the STEM/EDS measurements. Finally, the assistance of undergraduates Joseph H. Montoya, Jose J. Navarro, and Caroline Johnson in the laboratory is greatly appreciated.

References

[1] G.C. Bond, Catalysis by Metals, Academic Press, New York, 1962. p. 229.
[2] J. Regalbuto, Catalyst Preparation: Science and Engineering, CRC Press, 2007. p. 341.
[3] M. Chen, D. Kumar, C.-w. Yi, D.W. Goodman, Science 310 (2005) 291.
[4] M. Haruta, T. Kobayashi, H. Sano, N. Yamada, Chem. Lett. 16 (1987) 405.
[5] M. Haruta, M. Daté, Appl. Catal., A 222 (2001) 427.
[6] C.J. Baddeley, M. Tikhov, C. Hardacre, J.R. Lomas, R.M. Lambert, J. Phys. Chem. 100 (1996) 2189.
[7] N. Dimitratos, A. Villa, D. Wang, F. Porta, D. Su, L. Prati, J. Catal. 244 (2006) 113.
[8] M.D. Hughes, Y.-J. Xu, P. Jenkins, P. McMorn, P. Landon, D.I. Enache, A.F. Carley, G.A. Attard, G.J. Hutchings, F. King, E.H. Stitt, P. Johnston, K. Griffin, C.J. Kiely, Nature 437 (2005) 1132.
[9] J.K. Edwards, A.F. Carley, A.A. Herzing, C.J. Kiely, G.J. Hutchings, Faraday Discuss. 138 (2008) 225.
[10] C. Corti, R. Holliday, D. Thompson, Top. Catal. 44 (2007) 331.
[11] W.C. Ketchie, M. Murayama, R.J. Davis, J. Catal. 250 (2007) 264.
[12] G.J. Hutchings, Chem. Commun. (2008) 1148.
[13] A. Arcadi, Chem. Rev. 108 (2008) 3266.
[14] A.M. Venezia, V. La Parola, G. Deganello, B. Pawelec, J.L.G. Fierro, J. Catal. 215 (2003) 317.
[15] B. Pawelec, A.M. Venezia, V. La Parola, E. Cano-Serrano, J.M. Campos-Martin, J.L.G. Fierro, Appl. Surf. Sci. 242 (2005) 380.
[16] W. Hou, N.A. Dehm, R.W.J. Scott, J. Catal. 253 (2008) 22.
[17] A.M. Venezia, V. La Parola, V. Nicolì, G. Deganello, J. Catal. 212 (2002) 56.
[18] A. Corma, P. Serna, Science 313 (2006) 332.
[19] Y. Pluntke, L.A. Kibler, D.M. Kolb, Phys. Chem. Chem. Phys. 10 (2008) 3684.
[20] L. Prati, A. Villa, F. Porta, D. Wang, D. Su, Catal. Today 122 (2007) 386.
[21] D. Wang, A. Villa, F. Porta, D. Su, L. Prati, Chem. Commun. (2006) 1956.
[22] A. Villa, C. Campione, L. Prati, Catal. Lett. 115 (2007) 133.
[23] N. Dimitratos, F. Porta, L. Prati, Appl. Catal., A 291 (2005) 210.
[24] C.L. Bianchi, P. Canton, N. Dimitratos, F. Porta, L. Prati, Catal. Today 102–103 (2005) 203.

[25] N. Dimitratos, J.A. Lopez-Sanchez, J.M. Anthonykutty, G. Brett, A.F. Carley, R.C. Tiruvalam, A.A. Herzing, C.J. Kiely, D.W. Knight, G.J. Hutchings, Phys. Chem. Chem. Phys. 11 (2009) 4952.
[26] N. Dimitratos, J.A. Lopez-Sanchez, D. Morgan, A.F. Carley, R. Tiruvalam, C.J. Kiely, D. Bethell, G.J. Hutchings, Phys. Chem. Chem. Phys. 11 (2009) 5142.
[27] A.A. Herzing, A.F. Carley, J.K. Edwards, G.J. Hutchings, C.J. Kiely, Chem. Mater. 20 (2008) 1492.
[28] K.D. Beard, D. Borrelli, A.M. Cramer, D. Blom, J.W. Van Zee, J.R. Monnier, ACS Nano 3 (2009) 2841.
[29] K.D. Beard, J.W. Van Zee, J.R. Monnier, Appl. Catal., B 88 (2009) 185.
[30] S.S. Djokic, Mod. Aspect Electrochem. 35 (2002) 51.
[31] C.D. Iacovangelo, K.P. Zarnoch, J. Electrochem. Soc. 138 (1991) 983.
[32] M.T. Schaal, A.Y. Metcalf, J.H. Montoya, J.P. Wilkinson, C.C. Stork, C.T. Williams, J.R. Monnier, Catal. Today 123 (2007) 142.
[33] M.T. Schaal, A.C. Pickerell, C.T. Williams, J.R. Monnier, J. Catal. 254 (2008) 131.
[34] C. Contescu, A. Contescu, J.A. Schwarz, Chem. Rev. 95 (1995) 477.
[35] F.V. Hanson, M. Boudart, J. Catal. 53 (1978) 56.
[36] R.H. Doremus, J. Chem. Phys. 40 (1964).
[37] H.O. Ali, I.R.A. Christie, Gold Bull. 17 (1984) 118.
[38] S.D. Swan, E.L. Goswin, Met. Finish. 59 (1961) 52.
[39] Y. Okinaka, Electroless Plating of Gold and Gold Alloys, American Electroplaters and surface Finishers Society, Orlando, Florida, 1990. p. 415.
[40] R.K. Asher, Gold Bull. 13 (1980) 7.
[41] F. Simon, Gold Bull. 26 (1993) 14.
[42] J.R. Henry, Met. Finish. 105 (2007) 350.
[43] A.M. Weisberg. Gold Plating, Technic Inc., Providence, RI, 1994, p. 248.
[44] R.C. Weast, Handbook of Chemistry and Physics, CRC Press, Inc., Boca Raton, Florida, 1990. p. 151.
[45] J.E.A.M. Van den Meerakker, J. Appl. Electrochem. 11 (1981) 387.
[46] J.E.A.M. Van den Meerakker, J. Appl. Electrochem. 11 (1981) 395.
[47] E.J. O'Sullivan, Adv. Electrochem. Sci. Eng. 7 (2001) 225.
[48] Y. Okinaka, T. Osaka, Adv. Electrochem. Sci. Eng. 3 (1994) 55.
[49] I. Ohno, O. Wakabayashi, S. Haruyama, Electrochem. Soc. 132 (1985) 2323.
[50] A.M. Schwartzberg, T.Y. Olson, C.E. Talley, J.Z. Zhang, J. Phys. Chem. B 110 (2006) 19935.
[51] S. Basu, S. Pande, S. Jana, S. Bolisetty, T. Pal, Langmuir 24 (2008) 5562.
[52] C.R.K. Rao, D.C. Trivedi, Coord. Chem. Rev. 249 (2005) 613.
[53] G. Ertl, H. Knozinger, J. Weitkamp, Handbook of Heterogeneous Catalysis, VCH, 1997. p. 194.
[54] J.E. Benson, H.S. Hwang, M. Boudart, J. Catal. 30 (1973) 146.
[55] P.A. Webb, MIC Tech. Publ. (2003) 1.
[56] C.D. Iacovangelo, J. Electrochem. Soc. 138 (1991) 976.
[57] L.L. Sheu, Z. Karpinski, W.M.H. Sachtler, J. Phys. Chem. 93 (2002) 4890.
[58] A. Palazov, C.C. Chang, R.J. Kokes, J. Catal. 36 (1975) 338.
[59] J.B. Giorgi, T. Schroeder, M. Bäumer, H.-J. Freund, Surf. Sci. 498 (2002) L71.
[60] P. Gelin, A.R. Siedle, J.T. Yates, J. Phys. Chem. 88 (2002) 2978.
[61] X. Xu, D.W. Goodman, J. Phys. Chem. 97 (2002) 7711.
[62] S.S. Ashour, J.E. Bailie, C.H. Rochester, J. Thomson, G.J. Hutchings, J. Mol. Catal. A: Chem. 123 (1997) 65.
[63] J. Szanyi, W.K. Kuhn, D.W. Goodman, J. Vac. Sci. Technol. A 11 (1993) 1969.
[64] A.M. Bradshaw, F.M. Hoffmann, Surf. Sci. 72 (1978) 513.
[65] F. Skoda, M.P. Astier, G.M. Pajonk, M. Primet, Catal. Lett. 29 (1994) 159.
[66] E.L. Kugler, M. Boudart, J. Catal. 59 (1979) 201.
[67] M.G. Mason, Phys. Rev. B 27 (1983) 748.
[68] D.L. Weissman-Wenocur, P.M. Stefan, B.B. Pate, M.L. Shek, I. Lindau, W.E. Spicer, Phys. Rev. B 27 (1983) 3308.
[69] M. Boudart, M.A. McDonald, J. Phys. Chem. 88 (1984).
[70] L.B. Oritz-Soto, J.R. Monnier, M.D. Amiridis, Catal. Lett. 107 (2006) 13.
[71] I. Houruiti, M. Polanyi, Trans. Faraday Soc. 30 (1934) 1164.
[72] P.S. Cremer, G.A. Somorjai, J. Chem. Soc., Faraday Trans. 91 (1995) 3671.
[73] P.S. Cremer, X. Su, Y.R. Shen, G.A. Somorjai, J. Phys. Chem. 100 (1996) 16302.
[74] P.S. Cremer, X. Su, Y.R. Shen, G.A. Somorjai, J. Am. Chem. Soc. 118 (1996) 2942.
[75] C.H. Bartholomew, Appl. Catal., A 212 (2001) 17.